Environmental Science Nano

ROYAL SOCIETY OF CHEMISTRY

PAPER

View Article Online
View Journal | View Issue

Cite this: *Environ. Sci.: Nano*, 2023, **10**, 2578

pH-responsive copper-doped ZIF-8 MOF nanoparticles for enhancing the delivery and translocation of pesticides in wheat plants†

Chunli Xu, Lidong Cao, * Tingting Liu, Huiping Chen and Yuanbo Li*

Metal–organic framework (MOF)-based "nanopesticides" with pH-responsive performance have attracted increasing attention for application in sustainable agriculture. However, little attention has been paid to the impact of nanocarriers on the translocation of nanopesticides in plants. Herein, copper-doped ZIF-8 bimetallic MOF nanoparticles (Cu@ZIF-8) were prepared as nanocarriers by *in situ* fabrication of ZIF-8. Fludioxonil-loaded Cu@ZIF-8 (Flu@Cu@ZIF-8) could be constructed, and the loading content was 23.9%. The average particle size of Flu@Cu@ZIF-8 was ~80 nm. Flu@Cu@ZIF-8 exhibited acid-responsive release, with cumulative release of 79.5%, 69.9%, and 43.0% at pH values of 5, 7, and 9, respectively, after 48 h. Compared with free fludioxonil, Flu@Cu@ZIF-8 had similar percent inhibition against *Fusarium graminearum*, and the acute toxicity of fludioxonil against zebrafish could be reduced by up to 68% for Flu@Cu@ZIF-8 after 96 h of exposure. Confocal laser scanning microscopy showed that FITC-labeled Cu@ZIF-8 could be transported to all parts of a wheat plant from its roots. Flu@Cu@ZIF-8 exhibited stronger uptake and translocation in wheat plants, with a translocation factor 23–41% higher than that of fludioxonil alone. Overall, this work provides insights into the use of stimuli-responsive metal-doped MOF nanocarriers as pesticide-delivery systems in sustainable agriculture.

Received 15th May 2023,
Accepted 7th August 2023

DOI: 10.1039/d3en00300k

rsc.li/es-nano

Environmental significance

Improving the uptake and translocation of pesticides is a major scientific problem. The application of nanotechnology in pesticide loading is an effective way to help solve this problem. Herein, copper-doped ZIF-8 bimetallic MOF nanoparticles (Cu@ZIF-8) loaded with fludioxonil were prepared to obtain a pH-responsive controlled-release "nanopesticide" (Flu@Cu@ZIF-8). This nanopesticide showed similar fungicidal activity against *Fusarium graminearum* compared with fludioxonil alone, and slightly reduced toxicity to non-target organisms. Confocal laser scanning microscopy showed that FITC-labeled Cu@ZIF-8 could be transported to all parts of wheat plants from the roots. The high TF values of Flu@Cu@ZIF-8 implied that Cu@ZIF-8 could facilitate fludioxonil translocation in wheat plants. Our data demonstrate the potential application of MOF nanocarriers in improving pesticide utilization and reducing application times in sustainable agriculture.

1. Introduction

Pesticide application plays an important part in ensuring crop yields and meeting the needs of agricultural products for an increasing global population.[1,2] However, the utilization efficiency of conventional pesticide formulations for field applications is quite low. Only 10–15% of the applied pesticide can reach target sites due to drift, photolysis, microbial degradation, and runoff, and the percent uptake at the biological target is <0.1%.[3–4] The low efficiency of pesticide use has led to serious chemical waste and risks to the environment and human health.[5] Therefore, creating efficient and sustainable agrochemical formulations that are "green" is important for agricultural development. Rapid advances in nanotechnology have provided new strategies for the innovative preparation of pesticide formulations.[6–8] Nano-based pesticide formulations have been developed to protect crops thanks to their highly efficient pesticide loading, "intelligent" controlled release, enhanced biological activity, and environmentally friendly characteristics.[9–11] "Nanopesticides" with multifunctional features, such as on-demand or site specific-responsive release to various stimulus (*e.g.*, pH, light, glutathione, temperature) have drawn increasing attention.[12–14] Nanomaterials with special functions (*e.g.*, sensitivity to pH or heat) have received

State Key Laboratory for Biology of Plant Diseases and Insect Pests, Institute of Plant Protection, Chinese Academy of Agricultural Sciences, Beijing, 100193, P. R. China. E-mail: caolidong@caas.cn, liyuanbo@caas.cn; Tel: +86 10 62815938

† Electronic supplementary information (ESI) available. See DOI: https://doi.org/10.1039/d3en00300k

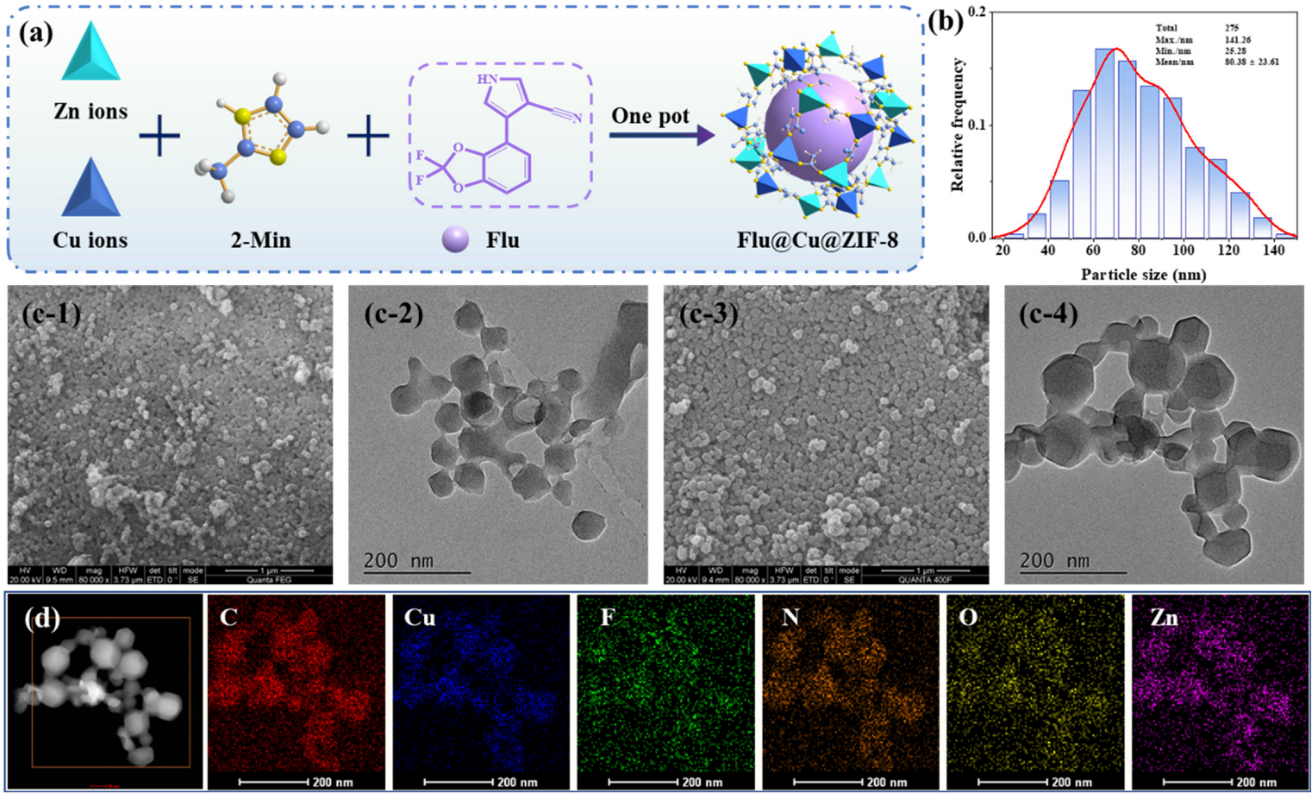

Fig. 1 The synthesis of Flu@Cu@ZIF-8 nanoparticles (a), size distribution (b), SEM and TEM images of nanoparticles (c) (1 and 2: Cu@ZIF-8; 3 and 4: Flu@Cu@ZIF-8), and elemental mapping (using energy-dispersive spectroscopy) of Flu@Cu@ZIF-8 (d).

particular attention in nanocarrier design for pesticides release.[15–17]

Metal–organic frameworks (MOFs) are a class of inorganic–organic hybrid porous crystalline materials formed by self-assembly of metal ions (clusters) and organic ligands.[18] MOFs are used widely as drug-release carriers because of their high efficiency of drug loading and versatile functions.[19,20] Recently, MOFs materials have been shown to be efficient pesticide-delivery systems and to have potential for agricultural applications.[21–24] Among MOFs materials, ZIF-8 is formed by coordination of the zinc ion (Zn^{2+}) and 2-methylimidazole. ZIF-8 has been designed as a pH-responsive carrier for the controlled delivery of agrochemicals.[14] Liang and colleagues reported that a ZIF-8-based nanocomposite loaded with prochloraz and 2,4-dinitrobenzaldehyde (a "pH jump" reagent) exhibited light-triggered pH-responsive release and excellent performance in controlling of sclerotinia disease.[25] Moreover, ZIF-8 can decompose into soluble zinc ions in water, which can serve as nutrients and reduce environmental pollution.[26] Besides, the imidazole group is an essential part of histidine.[27] Hence, ZIF-8 could be a green MOF material for the delivery of pesticides in agricultural applications.

ZIF-8 can be synthesized at room temperature, and it can absorb pesticides and store gas.[28,29] However, the absorbability and loading efficiency of ZIF-8 alone is low.[30] Studies have shown that modification of metal doping can endow ZIF-8 with excellent adsorption capacity.[31] For example, the adsorption capacity of copper-doped ZIF-8 for tetracycline hydrochloride increased by 4.8-times compared with that using unmodified ZIF-8.[29] Fe-doped ZIF-8 material has exhibited excellent magnetism as well as dual stimuli (pH and H_2S)-responsive release.[32] Bimetallic MOF nanoparticles loaded with a pesticide could be more effective for crop protection. Usually, Cu^{2+} is employed to fertilize and manage plant diseases in agriculture due to its recognized antifungal and antibacterial properties.[33] According to our previous study, copper-based nanocarriers loaded with a fungicide could improve antifungal activity.[34] Hence, copper-doped ZIF-8 might exhibit similar advantage to broaden the application of MOFs in plant protection. Studies have found that metal ions (*e.g.*, Cu^{2+} and Zn^{2+}) can influence accumulation of lipophilic organic compounds in plants.[35,36] However, whether copper-doped modification of ZIF-8 may have an impact on the translocation of pesticides in plants is not known, which is important for the selection of nanocarriers for pesticide delivery.

In this work, copper-doped ZIF-8 bimetallic MOF nanoparticles (Cu@ZIF-8) were constructed with an *in situ* fabrication process of ZIF-8 by a one-pot method. Fludioxonil (Flu) was used as a "model" pesticide because of its non-systemic property. Also, its poor translocation ability could help examination of the translocation potential of nanopesticides in plants.[37,38] Fludioxonil was incorporated into nanoparticles to

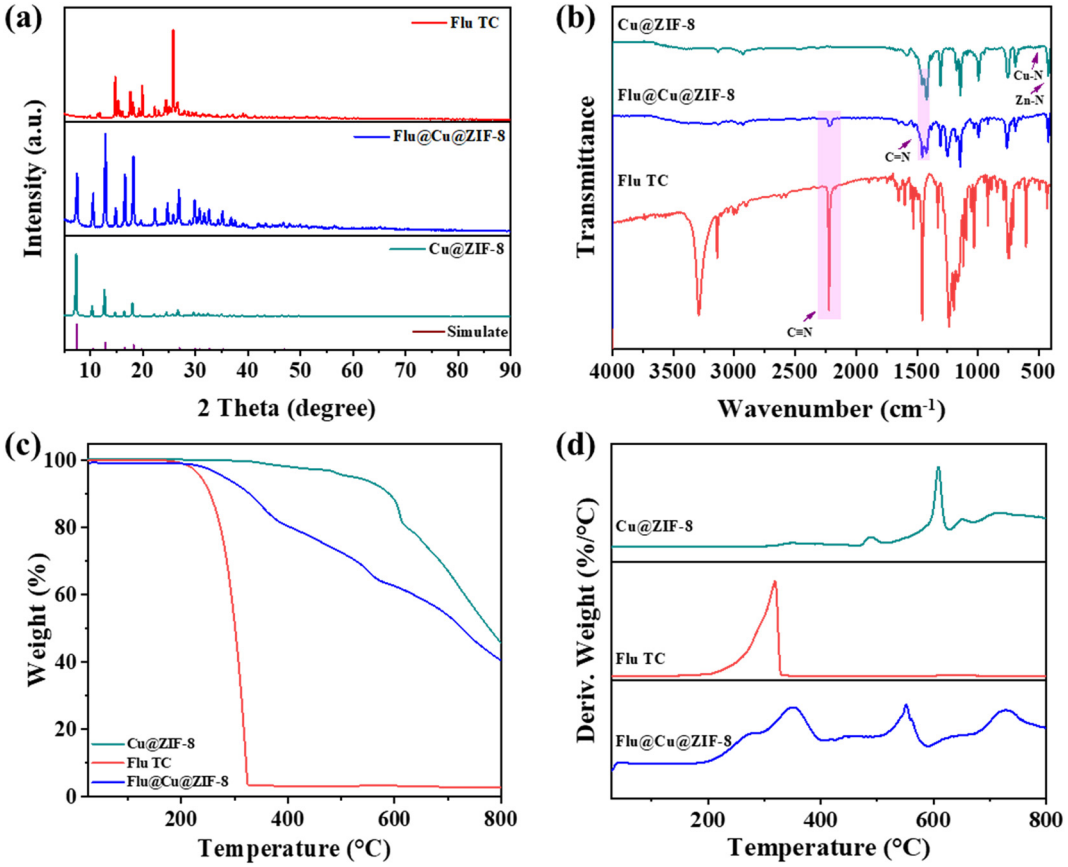

Fig. 2 XRD patterns (a), FT-IR spectroscopy (b), TGA (c), and DSC data (d) of Flu TC, Cu@ZIF-8, and Flu@Cu@ZIF-8.

prepare a pH-responsive nanopesticide: Flu@Cu@ZIF-8. The morphology, structure, and thermal stability of nanoparticles were characterized by scanning electron microscopy (SEM), X-ray diffraction (XRD), Fourier transform-infrared (FT-IR) spectroscopy, X-ray photoelectron spectroscopy (XPS), and thermogravimetric analysis (TGA). The loading content, release kinetics, antifungal effect, biosafety, and translocation in wheat plant were studied systemically. The findings in our study could provide deeper understanding of the performance of copper-doped ZIF-8 nanoparticles in facilitating the delivery and transfer of pesticides in plants.

2. Experimental section

2.1 Materials

Fludioxonil technique concentrate (Flu TC, 99%) was provided generously by Tianjin Jiuri Chemicals (Tianjin, China). $Cu(NO_3)_2{\cdot}2H_2O$, $Zn(NO_3)_2{\cdot}6H_2O$, phosphoric acid, and fluorescein isothiocyanate (FITC) isomer were obtained from Sinopharm Chemical Reagents (Beijing, China). The plant pathogen *Fusarium graminearum* was obtained from the Institution of Plant Protection within the Chinese Academy of Agricultural Sciences (Beijing, China). Deionized water was obtained from the Milli-Q™ water-purification system (Merck Millipore, Burlington, MA, USA). All other chemicals and reagents were commercially available and used as received.

2.2 Preparation of nanoparticles

Nanoparticles were synthesized according to a method reported previously with modification.[39] Briefly, 0.96 g of $Cu(NO_3)_2{\cdot}3H_2O$ and 4.8 g of $Zn(NO_3)_2{\cdot}6H_2O$ were added to a beaker containing 200 mL of deionized water. Then, 15 g of 2-methylimidazole and 6 g of fludioxonil were dissolved in 400 mL of methanol. The metal solution stated above was added to a mixed methanol solution of 2-methylimidazole and fludioxonil. The resulting mixture was stirred continuously for 30 min at a speed of 600 rpm. After centrifugation at 10 000 rpm for 5 min, the product was washed thrice with ethanol and then H_2O, respectively. The obtained solid product underwent vacuum freeze-drying and named Flu@Cu@ZIF-8. Cu@ZIF-8 was synthesized by the same procedure but without the addition of fludioxonil.

2.3 Synthesis of FITC-labeled Cu@ZIF-8

Briefly, 10 mg of FITC and 1.5 g of 2-methylimidazole were dissolved in 40 mL of methanol. Subsequently, 20 mL of deionized water containing 96 mg of $Cu(NO_3)_2{\cdot}3H_2O$ and 480 mg of $Zn(NO_3)_2{\cdot}6H_2O$ was added to the methanol solution. After stirring for 30 min, FITC-labeled Cu@ZIF-8 nanoparticles were centrifuged at 10 000 rpm for 5 min and washed by ethanol and water to remove fluorescence in the supernatant. Subsequently, the FITC-labeled Cu@ZIF-8

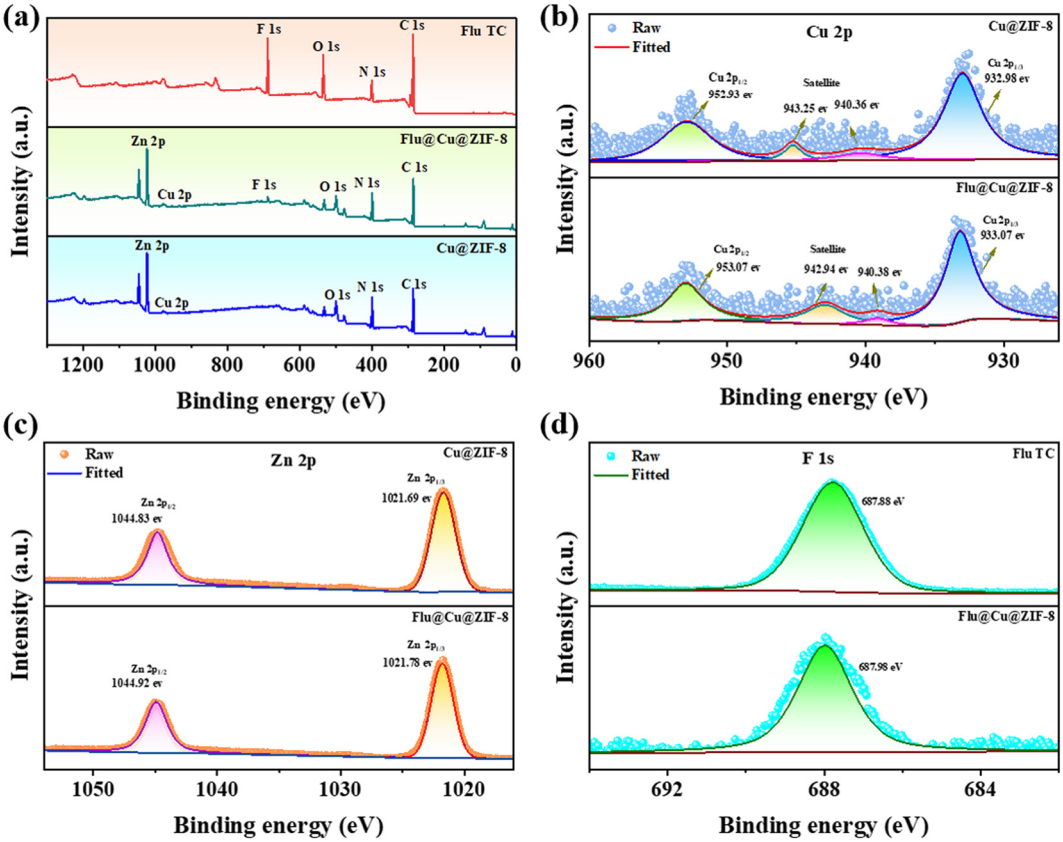

Fig. 3 Full XPS spectra of Flu TC, Cu@ZIF-8, and Flu@Cu@ZIF-8 (a). Cu 2p spectra (b). Zn 2p spectra (c). F 1s spectra (d).

nanoparticles were stored at room temperature and covered with aluminum foil to protect FITC from bleaching.

2.4 Characterization

The morphologies of nanoparticles were characterized using a scanning electron microscope (SU8000; Hitachi, Tokyo, Japan) operating at 10 kV, transmission electron microscope (Tecnai G2 and F20 S-TWIN; FEI, Hillsboro, OR, USA) with an accelerating voltage of 200 kV, and high-angle annular dark field scanning transmission electron microscopy (HAADF-STEM). The infrared spectra of nanoparticles were obtained through an FT-IR spectrometer (Bruker, Billerica, MA, USA). The crystal structure was acquired by an X-ray diffractometer (Micro; Rigaku, Tokyo, Japan) using Cu Kα radiation and k = 0.15418 nm. The distribution of elements was determined by XPS using a system from Kratos (Manchester, UK). The thermal stability of Flu TC, Cu@ZIF-8, and Flu@Cu@ZIF-8 were characterized using a thermogravimetric analyzer (Pyris Diamond; PerkinElmer, Waltham, MA, USA) from 20 °C to 800 °C at a heating rate of 15 °C min^{-1} under nitrogen flow. The size and zeta potential of samples were measured using a ZetaSizer Nano ZS Analyzer (BeNano 180 Zeta; Bettersize Instruments, Dandong, China).

2.5 Loading content of fludioxonil

We wished to determine the loading content of fludioxonil. Hence, 15 mg of Flu@Cu@ZIF-8 was weighed in a 25 mL flask with 5 mL of acetonitrile solution containing 100 μL of phosphoric acid. After 5 min of sonication, acetonitrile was added to the flask to make the volume reach 25 mL. The resulting solution was passed through a filter membrane (pore size = 0.22 μm). The amount of fludioxonil in nanoparticles was determined by high-performance liquid chromatography (HPLC) using the 1100-DAD system (Agilent Technologies, Santa Clara, CA, USA) with a TC-C_{18} reversed-phase column (5 μm, 4.6 × 150 mm; Agilent Technologies). Acetonitrile and an aqueous solution of 0.2% formic acid (v/v = 80 : 20) were used as the mobile phase at a flow rate of 1.0 mL min^{-1}. The detection wavelength was set at 226 nm and the injection volume was 5 μL. The linear regression equation of fludioxonil was $y = 0.0956x - 17.856$, and $R^2 = 0.999$. The loading content of fludioxonil was calculated using eqn (1):

$$\text{Loading content (\%)} = \frac{\text{weight of fludioxonil entrapped in nanoparticles}}{\text{weight of nanoparticles}} \times 100 \quad (1)$$

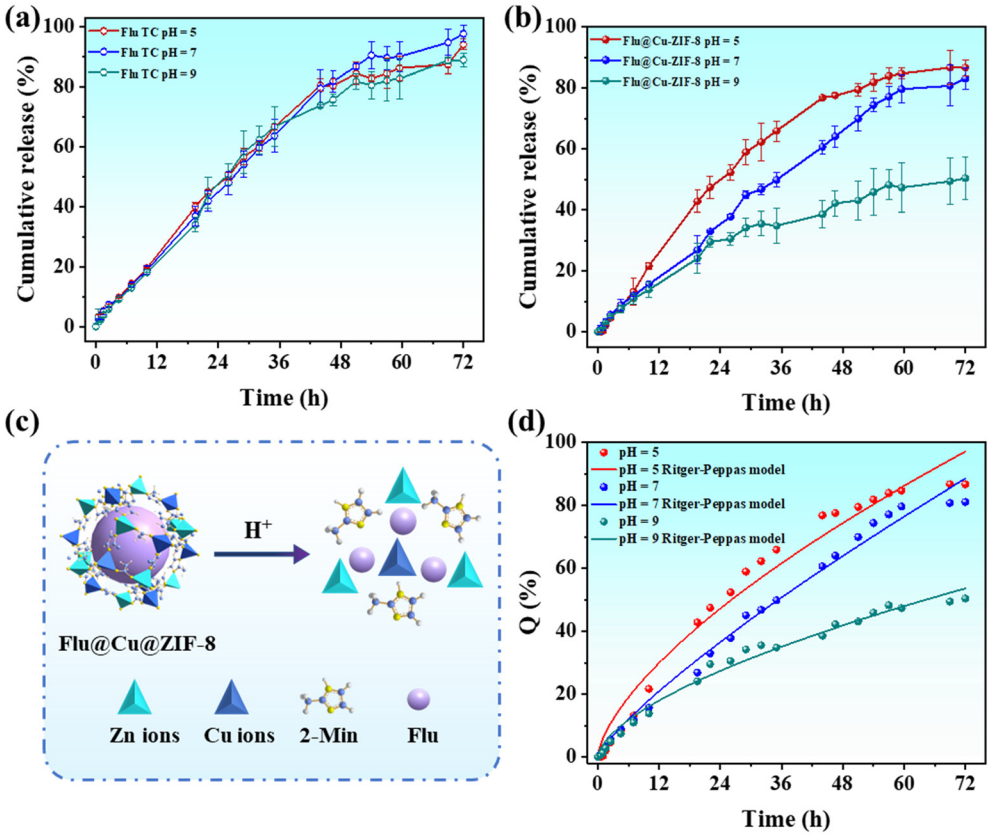

Fig. 4 Cumulative release of Flu TC (a) and Flu@Cu@ZIF-8 (b). Potential release mechanism of Flu@Cu@ZIF-8 at different pH conditions (c). Fitting curve of the Ritger–Peppas model (d). Results are the mean ± standard deviation (n = 3).

Table 1 Fitting results for fludioxonil-release curves of samples at different pH conditions

		5		7		9	
pH	Fitting model	Kinetic equation	R^2	Kinetic equation	R^2	Kinetic equation	R^2
Flu TC	Zero-order	$Q = 0.01546t$	0.9294	$Q = 0.01593t$	0.9597	$Q = 0.01501t$	0.9282
	First-order	$Q = 1 - e^{0.03061t}$	0.9882	$Q = 1 - e^{0.0312t}$	0.9736	$Q = 1 - e^{0.02869t}$	0.9899
	Ritger–Peppas	$Q = 0.05429t^{0.68142}$	0.9809	$Q = 0.04262t^{0.75049}$	0.9869	$Q = 0.0519t^{0.68533}$	0.9782
	Higuchi	$Q = 0.10802t^{1/2}$	0.9529	$Q = 0.11047t^{1/2}$	0.9409	$Q = 0.10481t^{1/2}$	0.9491
Flu@Cu@ZIF-8	Zero-order	$Q = 0.01512t$	0.9105	$Q = 0.01359t$	0.9939	$Q = 0.00849t$	0.8966
	First-order	$Q = 1 - e^{0.02998t}$	0.9946	$Q = 1 - e^{0.02256t}$	0.9717	$Q = 1 - e^{0.01164t}$	0.9644
	Ritger–Peppas	$Q = 0.05861t^{0.65633}$	0.9743	$Q = 0.02841t^{0.8045}$	0.9906	$Q = 0.03943t^{0.61003}$	0.9786
	Higuchi	$Q = 0.1059t^{1/2}$	0.9522	$Q = 0.09322t^{1/2}$	0.9187	$Q = 0.\ 05978t^{1/2}$	0.9737

2.6 Kinetics of controlled release

A typical release system was prepared by suspending 20 mg of Flu@Cu@ZIF-8 in 200 mL of acetonitrile/water (30 : 70, v/v) buffer solution with 0.5% Tween-80 at pH values of 5, 7, and 9. The release system was maintained at 25 ± 1 °C in a shaker (Shanghai Yiheng Scientific Instruments, Shanghai, China) at a rotation speed of 200 rpm. Then, at specified time intervals, 0.7 mL of the mixture was sampled for analyses. To keep the total volume of the solution constant, 0.7 mL of fresh solution was added. The concentration of fludioxonil in the solution was determined by HPLC. The cumulative release was calculated using the following equation:

$$E_r = \frac{V_e \sum_{i=0}^{n-1} C_i + V_0 C_n}{m_{\text{pesticide}}} \times 100\% \quad (2)$$

where E_r is the cumulative release (%) of fludioxonil from nanoparticles; V_e is the volume of the release medium taken at a given time interval (V_e = 0.7 mL); V_0 is the volume of release solution (200 mL); C_n (mg mL^{-1}) is the fludioxonil concentration in the release medium at time n; $m_{\text{pesticide}}$ (mg) is the total amount of fludioxonil loaded in nanoparticles.

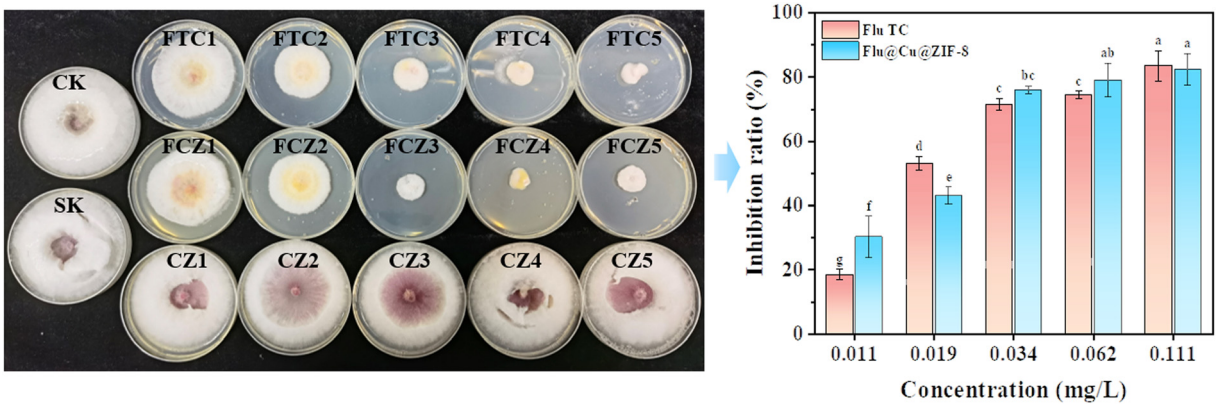

Fig. 5 Images showing the fungicidal activity of Flu TC (FTC), Flu@Cu@ZIF-8 (FCZ), and Cu@ZIF-8 (CZ, without fludioxonil) against *F. graminearum* for the corresponding concentrations of fludioxonil (1–5 means 0.011–0.111 mg L^{-1}), blank control (CK), and solvent blank (SK) after 5 days of treatment.

The release kinetics of fludioxonil from nanoparticles was analyzed through various models: Zero-order, first-order, Ritger–Peppas, and Higuchi:[34]

$$\text{Zero-order: } Q = kt$$

$$\text{First order: } Q = 1 - e^{-kt}$$

$$\text{Ritger–Peppas: } Q = kt^{n}$$

$$\text{Higuchi: } Q = kt^{1/2}$$

where Q_t is the cumulative release of fludioxonil at time t; k is a kinetic constant; n indicates the release mechanism; $n < 0.43$, $0.43 < n < 0.85$, and $n \geq 0.89$ represent Fickian diffusion, non-Fickian (or anomalous) diffusion, and zero-order transport, respectively.

2.7 Bioactivity test against *F. graminearum*

The bioactivities of Flu TC, Cu@ZIF-8, and Flu@Cu@ZIF-8 against *F. graminearum* were tested using a method based on the growth rate of mycelia. Flu TC was dissolved in dimethyl sulfoxide as a stock solution at a concentration of 2000 mg L^{-1}. Flu@Cu@ZIF-8 was dispersed in sterile water with the assistance of ultrasound to obtain a nanosuspension. A series of concentrations from 0.011 to 0.11 mg L^{-1} of Flu TC (or Flu@Cu@ZIF-8) was mixed with sterilized potato dextrose agar (PDA). Then, mycelial disks (5 mm in diameter) of *F. graminearum* were grown on PDA media. The test was carried out in triplicate. All PDA media were set at 25 °C in darkness for 5 days. The diameter of a mycelium in a colony was measured by the criss-cross method. Pathogenic inhibition was determined as: (colony diameter of control − colony diameter of treatment)/(colony diameter of control − diameter of mycelial disks) ×100%.

Table 2 LC_{50} values of Flu TC and Flu@Cu@ZIF-8 towards zebrafish

Code		LC_{50} (mg L^{-1})		R^2
Flu TC	24 h	0.8330	$y = 0.4 + 1.81x$	0.262
	48 h	0.3670	$y = 5.38 + 12.41x$	0.900
	72 h	0.3550	$y = 4.91 + 11.56x$	0.803
	96 h	0.3520	$y = 5.36 + 12.3x$	0.849
Flu@Cu@ZIF-8	24 h	0.7560	$y = 1.27 + 8.34x$	0.532
	48 h	0.6010	$y = 0.85 + 6.02x$	0.899
	72 h	0.5970	$y = 0.81 + 5.67x$	0.849
	96 h	0.5920	$y = 0.79 + 5.39x$	0.739

2.8 Acute toxicity to adult zebrafish

Zebrafish (*Danio rerio*) was selected as model non-target animal to evaluate the acute toxicity of Flu@Cu@ZIF-8 to aquatic organisms. Ten tails of adult zebrafish of similar size (2.5 ± 0.5 cm) were used for each treatment. Flu TC was dissolved in acetone as a stock solution at a concentration of 9000 mg L^{-1}. Flu@Cu@ZIF-8 was dispersed in water with the assistance of ultrasound to obtain a nanosuspension. The concentration of fludioxonil was set at 0.248–0.433 mg L^{-1} for Flu TC and 0.397–0.686 mg L^{-1} for Flu@Cu@ZIF-8, which was diluted with water. The death of zebrafish was recorded at 24, 48, 72, and 96 h according to Organization for Economic Co-operation and Development guidelines.[40] Each experiment was repeated three times. The median lethal concentration (LC_{50}) was calculated by probit analyses.

2.9 Germination and cultivation of wheat seeds

Wheat seeds (Nongda 202, China) were sterilized in 2–3% hypochlorite solution for 15 min, rinsed thoroughly with deionized water, followed by imbibing in deionized water for 16 h. Afterwards, the seeds were germinated in a seedling tray (made of polyvinyl chloride) for 4 days. Subsequently, uniform-size seedlings were transferred into 1 L glass containers (each container had 24 wheat seedlings) wrapped with foil paper with one-quarter strength of Hoagland solution. Plants were cultivated at an ambient temperature

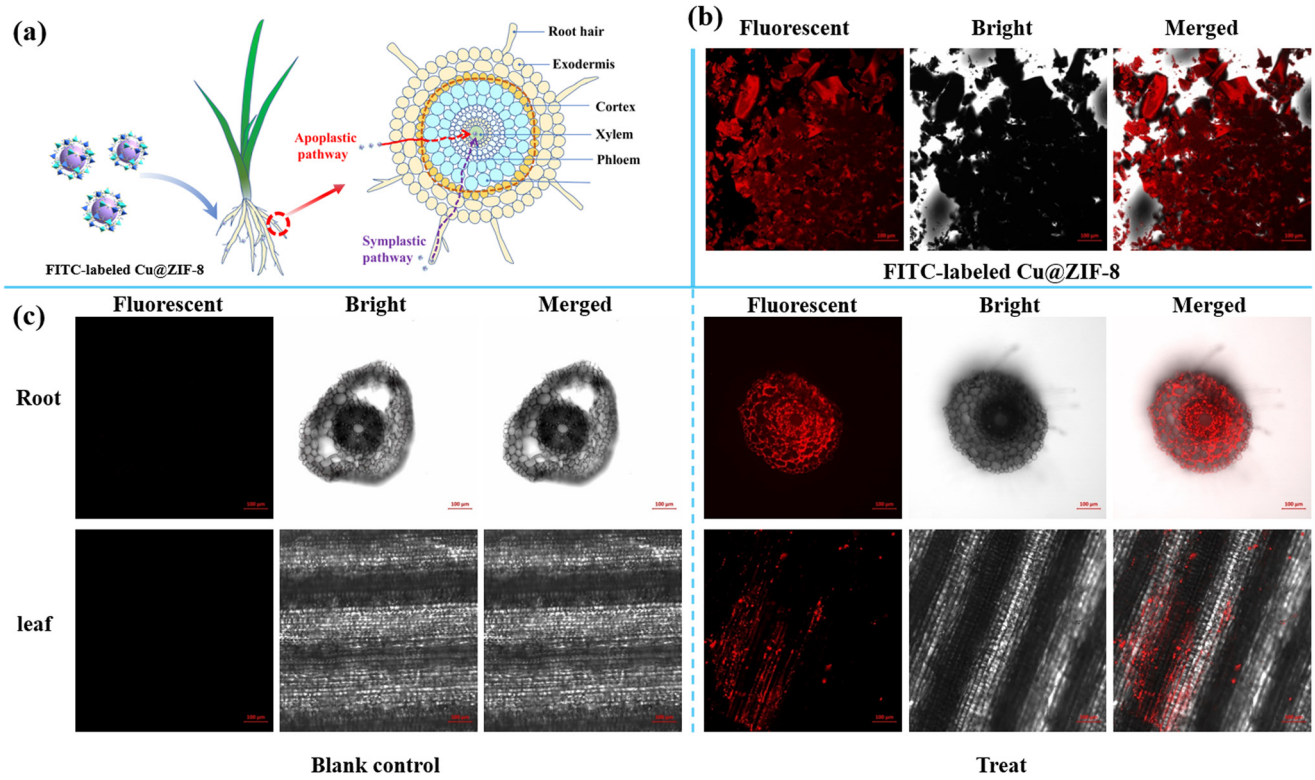

Fig. 6 Uptake pathway in wheat plants after root treatment by FITC-labeled Cu@ZIF-8 (a) (schematic). Confocal laser scanning image of FITC-labeled Cu@ZIF-8 (b) as well as the root and leaf of a wheat plant (c).

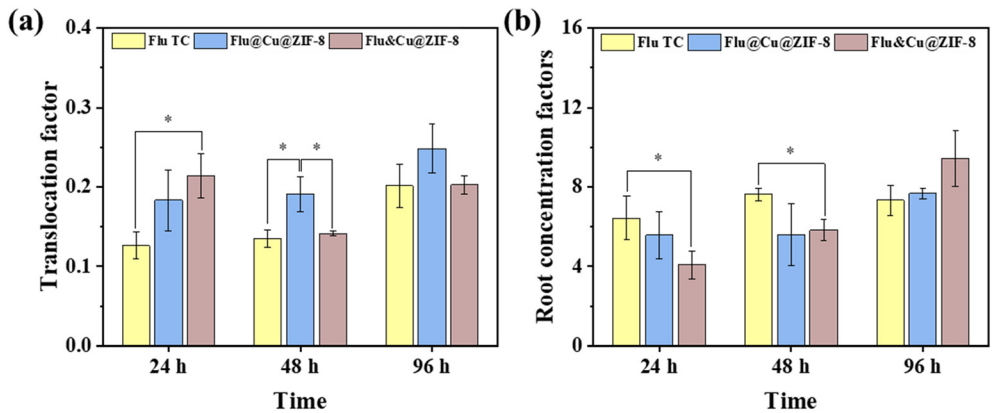

Fig. 7 Translocation factor (a) and root concentration factor (b) of fludioxonil in wheat plants by three types of treatment.

(25 ± 2 °C). The Hoagland solution was replaced every 3 days for each treatment to maintain sufficient nutrients for plant growth.

2.10 Uptake of nanoparticles by wheat plants

FITC-labeled Cu@ZIF-8 was used to explore the uptake and distribution of nanoparticles in wheat plants. Briefly, 1 week-old wheat plants were exposed to 5 mL of an aqueous suspension spiked with FITC-labeled Cu@ZIF-8 at 1 mg mL^{-1}. After treatment for 2 days, wheat roots and leaves were sampled for imaging with a confocal laser scanning microscope (LSM 880; Zeiss, Wetzlar, Germany) at an excitation wavelength of 488 nm.

2.11 Uptake and translocation of pesticide in wheat plants

After 14 days of growth of wheat seedlings, plants were transferred to a 1 L glass container containing 1 L of one-quarter strength of Hoagland solution. Nanoparticles loaded with fludioxonil were spiked in the solution at 1 mg L^{-1}. Four controls were included: (1) a pesticide-free control (plant only), (2) physical mixture solution of Flu TC with Cu@ZIF-8 nanoparticles, (3) Flu TC solution, and (4) control blank. The

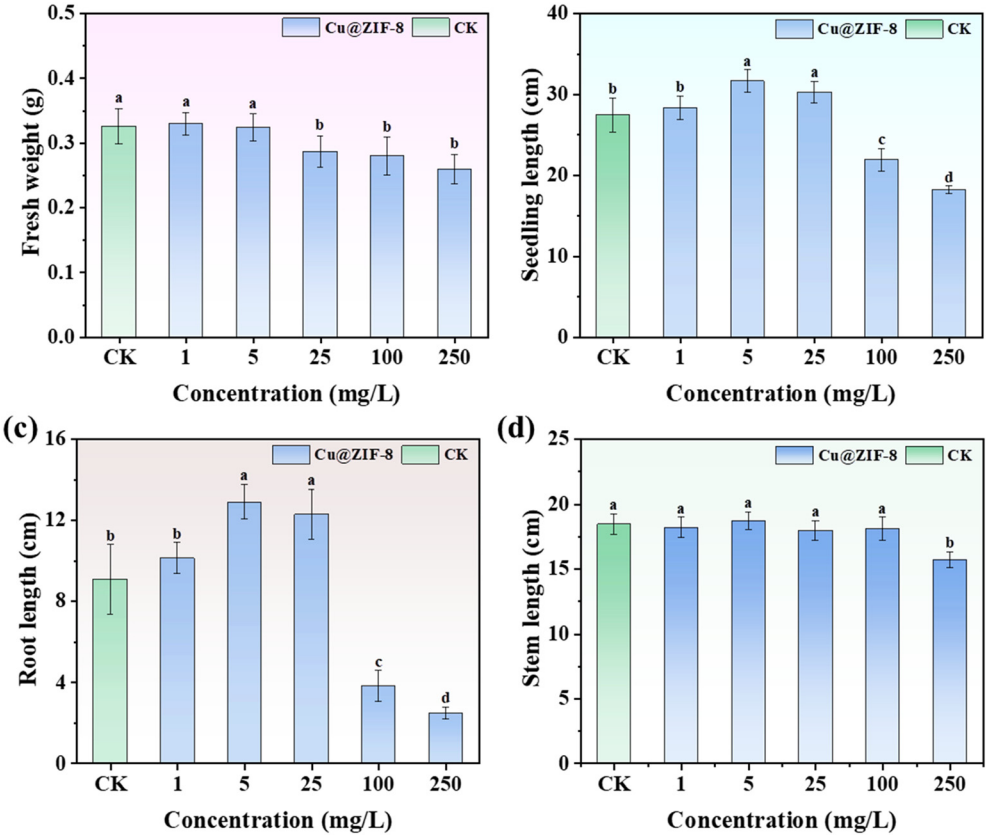

Fig. 8 Effects of root treatment of Cu@ZIF-8 on fresh weight (a), seedling length (b), root length (c), and stem length (d) of wheat plants. Different letters indicate a significant difference according to ANOVA ($P < 0.05$).

relative humidity was maintained at 60–70% with a light: dark cycle of 14 : 10 h. All exposure and control experiments were carried out in triplicate. Plant samples were collected after 24, 48, or 96 h of growth. Then, plant samples were rinsed with deionized water and divided into roots and shoots. The roots, shoots, and solution were collected for pesticide analyses. All the samples were stored at −20 °C prior to analyses. The root concentration factor (RCF) and translocation factor (TF) were calculated using the following equation:[41,42]

$$\mathrm{RCF} = C_{\mathrm{root}}/C_{\mathrm{water}}$$

$$\mathrm{TF} = C_{\mathrm{shoot}}/C_{\mathrm{root}}$$

where C_{root}, C_{shoot}, and C_{water} are the fludioxonil concentration in samples of the root, shoot, and solution, respectively (ng g^{-1} or ng mL^{-1}).

2.12 Sample analyses

A modified QuEChERS method was employed for fludioxonil extraction. Samples were quantified using ultra-high performance liquid chromatography–tandem mass spectrometry (UHPLC–MS/MS). More details of the method and HPLC-MS/MS parameters are described in the ESI† and Table S1. The recovery of fludioxonil in samples of roots, shoots, and hydroponic solution ranged from 87.3% to 106.3%, with relative standard deviation (RSD) values <16.21 (Table S2†). Matrix-matched solutions were prepared by adding a stock solution of fludioxonil to blank matrix extractions, and good linearity was obtained ($R^2 > 0.9916$) (Table S3†).

2.13 Biosafety assay of Cu@ZIF-8 nanoparticles against wheat plants

Two week-old wheat seedlings of similar size were transferred to a 50-mL beaker containing 30 mL of one-quarter strength of Hoagland solution with varying concentrations of Cu@ZIF-8 (0, 1, 5, 25, 100, or 200 mg L^{-1}) for 10 days. Each beaker was wrapped in tin foil. Each treatment had three replicates. Seedlings were incubated with a 14 h/10 h light/dark cycle at room temperature (25 ± 1 °C). The seedling length and fresh weight of the collected seedling samples were measured.

2.14 Statistical analyses

Statistical analyses were undertaken using SPSS 26.0 (IBM, Armonk, NY, USA). A significant difference in data was analyzed by one-way analysis of variance (ANOVA) ($p < 0.05$)

and expressed as the mean ± standard error of the mean for all experiments.

3. Results and discussion

3.1 Preparation and characterization of nanoparticles

Copper-doped Flu-loaded ZIF-8 nanoparticles (Flu@Cu@ZIF-8) were constructed following the synthetic process illustrated in Fig. 1a. The one-pot strategy facilitated the preparation of Flu@Cu@ZIF-8 on a scale. The average size (using Nano Measurer software) of Cu@ZIF-8 and Flu@Cu@ZIF-8 was determined to be 66.94 ± 10.31 nm and 80.38 ± 23.61 nm, respectively (Fig. 1b and S1†). Cu@ZIF-8 nanoparticles showed a well-defined truncated rhombic dodecahedron structure, which was consistent with the typical morphology of ZIF-8 (Fig. S2†). SEM and TEM images demonstrated the shape of ZIF-8 to be retained, as reported previously,[39] indicating that copper and encapsulated fludioxonil did not change the shape of ZIF-8 (Fig. 1c). As shown by elemental mapping using energy-dispersive spectroscopy, the distribution of copper and fluorine confirmed encapsulation of fludioxonil into Cu@ZIF-8 (Fig. 1d).

XRD was used to analyze the crystal structure of nanoparticles. As shown in Fig. 2a, the positions of the peaks of Cu@ZIF-8 and Flu@Cu@ZIF-8 were the same as the simulated curve of ZIF-8. Hence, the crystal structure of the prepared material was not disturbed by copper doping and pesticide loading. This was confirmed by infrared spectroscopy (Fig. 2b). The characteristic peaks of M–N (Cu–N and Zn–N) stretching and C═N bending were observed in Cu@ZIF-8 and Flu@Cu@ZIF-8 (Fig. S3†), which is in agreement with earlier reports.[43–44] Moreover, peaks at 2200 cm^{-1} corresponding to the C≡C group of fludioxonil in Flu@Cu@ZIF-8 suggested that fludioxonil and Cu@ZIF-8 did not change the chemical structure of the respective substances.

TGA was carried out to investigate the thermal decomposition of nanoparticles under N_2 flow. As shown in Fig. 2c, a rapid weight-loss step of 100% from ~220 °C to ~320 °C indicated that the structure of fludioxonil was unstable at temperatures higher than 200 °C. For Cu@ZIF-8, a weight-loss step in the range 300–520 °C could be attributed to decomposition of the organic ligands in Cu@ZIF-8.[45] A *plateau* in the differential scanning calorimetry (DSC) curve of Cu@ZIF-8 above 520 °C indicated that Cu@ZIF-8 might have decomposed completely and transformed into inorganic ZnO and CuO (Fig. 2d).[43] Conversely, a gradual weight loss occurred in Flu@Cu@ZIF-8 from 200 °C to 800 °C, which was attributed mainly to the slow decomposition of fludioxonil and organic ligands in nanoparticles. These results indicated that Cu@ZIF-8 could improve the thermal stability of fludioxonil.

XPS was employed to determine the elemental composition of samples (Fig. 3). The characteristic elemental peak of Cu@ZIF-8 in addition to the F 1s peak at 698.9 eV indicated that fludioxonil had been loaded with Cu@ZIF-8. The high resolution of Cu 2p, Zn 2p, F 1s, and C 1s were analyzed to investigate the interaction mechanism between fludioxonil and Cu@ZIF-8. Peaks at 952.93 eV and 932.98 eV were assigned to Cu $2p_{1/2}$ and Cu $2p_{3/2}$ of Cu^{2+}, respectively[46] (Fig. 3b). The satellite peak at 943.25 eV and 940.36 eV also indicated the characteristics of Cu^{2+}. The Zn 2p spectra at 1021.69 eV and 1044.83 eV (Fig. 3c) were attributed to the characteristic binding energies of Zn $2p_{3/2}$ and Zn $2p_{1/2}$, which was concordant with the literature.[47,48] As indicated in Fig. S4,† the C 1s spectrum of Cu@ZIF-8 exhibited peaks at 284.59 eV and 285.46 eV, which were ascribed to C═C, C≡C, C–N, and C═N of the imidazole. The C 1s spectrum possessed a new peak at 292.98 eV for C≡N (Fig. S5 and S6†), suggesting that fludioxonil was stable in Flu@Cu@ZIF-8. Furthermore, the spectra of F 1s (Fig. 3d) observed at ~687.8 eV provided additional evidence of the encapsulation of fludioxonil within Cu@ZIF-8.

3.2 Loading efficiency and controlled-release profiles of pesticide

The copper doping of ZIF-8 could affect the loading content of cargo molecules. The loading content of fludioxonil in Flu@Cu@ZIF-8 was determined to be 23.9 ± 1.2%, which was higher than that of Flu@ZIF-8 (15.8 ± 1.4%). This finding was probably due to copper doping, which affected the surface area and pore structure of ZIF-8.[29] The cumulative-release profile of fludioxonil at pH values of 5, 7 and 9 was investigated to evaluate the release behaviors of nanoparticles. Fig. 4 shows that Flu TC did not have sensitive release in the pH ranges tested, whereas Flu@Cu@ZIF-8 demonstrated obvious pH-responsive release. As shown in Fig. 4b, the cumulative amount of fludioxonil released reached 79.5% after 48 h at pH 5, and 69.9% and 43.0% of fludioxonil was released at pH 7 and 9, respectively. Under acidic conditions, the coordination between zinc ions and imidazolate rings can be broken due to protonation of 2-methylimidazole linkers, thereby ensuring the acid-sensitive characteristic of ZIF-8.[49,50] With regard to the composition of Cu@ZIF-8, copper ions substituted for zinc ions in ZIF-8, but the crystal structure of Cu@ZIF-8 was the same as ZIF-8. Therefore, Cu@ZIF-8 continued to have the acid-sensitive characteristic. These results demonstrated that Flu@Cu@ZIF-8 had pH-responsive release behavior. Hence, Flu@Cu@ZIF-8 could selectively target plant pathogens in an acidic microenvironment (*e.g.*, plant phloem sap).[51]

Four models were used to investigate the possible release mechanism of fludioxonil at pH 5, 7, and 9. According to the correlation coefficient (R^2) of fitted equations, the data for fludioxonil release from Flu TC had the best fit using the first-order model. For Flu@Cu@ZIF-8, the Ritger–Peppas equation described the release behavior of fludioxonil. The release exponent (n) was used to evaluate the diffusion mechanism.[52] The n value of Flu@Cu@ZIF-8 was between 0.45 and 0.89, which meant that the release behavior was

non-Fickian diffusion. All fitted parameter values are summarized in Table 1.

3.3 Activity of flu@cu@ZIF-8 against *F. graminearum*

F. graminearum is a major pathogen that causes a devastating disease in cereal crops known as "Fusarium head blight". *F. graminearum* can promote a plant to produce toxic secondary metabolites, which brings economic losses in farming and health impacts on humans.[53] An acidic environment is beneficial for the growth of *F. graminearum* and contributes to the production of secondary metabolites such as deoxynivalenol. Depending on the acid-triggered release of Flu@Cu@ZIF-8, fludioxonil could be released to control pathogens effectively. As shown in Fig. 5, at a fludioxonil concentration <0.03 mg L^{-1}, the fungicidal activity of Flu@Cu@ZIF-8 was slightly lower than that of Flu TC. This finding might have been due to the time required to release the active ingredient from Flu@Cu@ZIF-8, thereby resulting in a lower concentration of free fludioxonil in PDA than that of Flu TC. The half-maximal effective concentration (EC_{50}) of Flu TC and Flu@Cu@ZIF-8 was 0.041 mg L^{-1} and 0.038 mg L^{-1}, respectively, indicating that similar fungicidal activity could be achieved for Flu TC and Flu@Cu@ZIF-8. All the concentrations of Cu@ZIF-8 tested led to no fungicidal activity.

3.4 Acute toxicity towards adult zebrafish

Table 2 reveals that acute toxicity of fludioxonil against zebrafish varied with time after loading into Cu@ZIF-8. After 24 h of treatment, the LC_{50} value of Flu TC towards zebrafish was 0.833 mg L^{-1}, and the LC_{50} value of Flu@Cu@ZIF-8 was 0.756 mg L^{-1}. After 96 h of exposure, the LC_{50} value of Flu@Cu@ZIF-8 towards zebrafish could increase by 68% that of Flu TC. This observation could be ascribed to the slow release of the active ingredient from nanoparticles. Hence, the bioavailable concentration of fludioxonil in Flu@Cu@ZIF-8 solution was lower than that of Flu TC solution. The LC_{50} values of Flu TC and Flu@Cu@ZIF-8 were less than 1 mg L^{-1} and ranked as "high toxicity" against zebrafish. However, the acute toxicity of fludioxonil could be reduced due to the slow release of the active ingredient after fludioxonil loading into Cu@ZIF-8.

3.5 Uptake of FITC-labeled Cu@ZIF-8 nanoparticles in wheat plants

Nanoparticles can enter plants through permeation, endocytosis, and other pathways.[54] The uptake and translocation of Cu@ZIF-8 nanoparticles were visualized by confocal laser scanning microscopy. As shown in Fig. 6, FITC-labeled Cu@ZIF-8 showed a clear fluorescence signal in plant tissues under a laser-excitation wavelength of 488 nm. This result indicated that FITC-labeled Cu@ZIF-8 could be absorbed by the roots and transferred to the upper parts of a wheat plant. FITC-labeled Cu@ZIF-8 was first absorbed on the root surface, and its surface chemistry could be modified by organic acids produced by root exudates,[55,56] which helped to reduce the aggregation of nanoparticles and entrance into the plant, respectively. As shown in Fig. S7,† the negative potential of a FITC-labeled Cu@ZIF-8 test solution changed from −12 mV to −19 mV after 2 days of treatment.

3.6 Uptake and translocation of fludioxonil in wheat plants

The translocation factor (TF) was used to assess the translocation ability of a pesticide from the root to shoot. TF < 1 denotes poor translocation from the roots to above-ground tissues.[42] As presented in Fig. 7a, the TF of Flu TC was in the range 0.14–0.2, suggesting that fludioxonil accumulated preferentially in the roots of a wheat plant. The TF values of Flu@Cu@ZIF-8 and physical mixing nanoparticles (Flu&Cu@ZIF-8) were also <1. However, after 48 h of exposure, the TF value of Flu@Cu@ZIF-8 was 23–41% higher than those of Flu&Cu@ZIF-8 and Flu TC, implying that nanoparticles could facilitate the upward translocation of fludioxonil in a wheat plant. Cu@ZIF-8 at a small scale could enter the plant readily. Hence, Cu@ZIF-8 might act as a carrier to enhance the upward translocation of fludioxonil in plants, and increase the protective property of the active ingredient. After 96 h of exposure, the RCF value of fludioxonil in roots was ranked Flu&Cu@ZIF-8 (9.4 g g^{-1}) > Flu@Cu@ZIF-8 (7.6 g g^{-1}) ≈ Flu TC (7.3 g g^{-1}) (Fig. 7b). Hence, Cu@ZIF-8-encapsulated fludioxonil did not influence fludioxonil accumulation in the roots significantly. The uptake and accumulation of pesticides in plants are complex processes. The different trends of accumulation in the roots among three treatments might have been due to the slow release of fludioxonil from nanoparticles. Our results indicated that the uptake and accumulation of fludioxonil in plants were determined by the plant, exposure time, and chemical properties, but also by the nanoparticle itself in terms of bioavailability regulation.

3.7 Biosafety evaluation against wheat plants

To examine the regulatory effect of Cu@ZIF-8 on plant growth, wheat plants were cultured with Cu@ZIF-8 to study the variance in fresh weight, seedling height, stem length, and root length. As shown in Fig. 8a, there was no obvious inhibition of the fresh weight of plants treated with Cu@ZIF-8 at a low exposure concentration (<5 mg L^{-1}). However, the fresh weight of wheat plants treated with Cu@ZIF-8 decreased by 12.0–20.4% with an increasing test concentration (25–100 mg L^{-1}). The effect of Cu@ZIF-8 on seedling length (Fig. 8b) and root length (Fig. 8c) showed a trend of initially promotion (1–25 mg L^{-1}) and then inhibition (25–100 mg L^{-1}) with an increasing test concentration. The seedling length and root length reached up to 15.3% and 42.1% higher than that of the blank control at 5–25 mg L^{-1}, which might have been due to supplementation of nutrient elements by Cu@ZIF-8 (*e.g.*, Cu or Zn). However, at <100 mg L^{-1}, the root length decreased significantly to 42.0% compared with the blank control.

The negative impact of nanoparticles on plant growth was concentration-dependent, as documented previously.[57] Tiwari *et al.* reported that low doses of CuO-NPs (5–50 μM) promoted the growth of rice seedlings, whereas high doses (100–500 μM) reduced the growth of seedlings.[58] The negative impacts on plant growth are likely related to the excessive formation of reactive oxygen species (ROS) induced by nanoparticles.[59,60] Excessive levels of ROS could result in oxidative damage (and even cell death). Moreover, the electrostatic charges, osmotic stress, interfacial tension, and steric interaction associated with nanoparticles, as well as cellular penetration into plants, may also result in damage to plants.[60] Our results indicated that MOF materials could promote plant growth as nutrients by application of doses at low concentrations. Furthermore, the influence of Flu@Cu@ZIF-8 showed no significant difference in fresh weight, seedling height, stem length, or root length with that of Flu TC at a high test concentration (Fig. S8†), which suggested that Cu@ZIF-8 nanoparticles did not increase the toxicity or side-effects of fludioxonil on wheat-plant growth. Therefore, Cu@ZIF-8 could be used at an acceptable concentration as a carrier for precise pesticide delivery to protect crop growth.

4. Conclusions

Copper-doped ZIF-8 bimetallic MOF nanoparticles were designed with a simple *in situ* fabrication process of ZIF-8 by a one-pot method, and were used as nanocarriers to control the delivery and release of fludioxonil. Flu@Cu@ZIF-8 demonstrated pH-responsive release due to the protonation of 2-methylimidazole linkers in an acidic environment. Of the four release models, the Ritger–Peppas model could explain the release mechanism of Flu@Cu@ZIF-8. Results suggested that non-Fickian diffusion controlled the release of fludioxonil from Flu@Cu@ZIF-8 at pH 5–9. The plate method indicated that Flu@Cu@ZIF-8 had a similar level of inhibition against *F. graminearum*. Compared with control treatment, the nanocarrier Cu@ZIF-8 could promote the seedling length and root length of wheat plants by up to 15.3% and 42.1%, respectively, upon treatment at 5–25 mg L^{-1}. The higher TF values of Flu@Cu@ZIF-8 implied that Cu@ZIF-8 could facilitate fludioxonil translocation in wheat plants. The adverse effect of fludioxonil against zebrafish could be reduced slightly after loading into Cu@ZIF-8. The copper-doped ZIF-8 MOF nanocarrier loaded with fludioxonil could improve the percent utilization of fludioxonil through pH-responsive controlled release and enhanced translocation in plants.

Author contributions

Chunli Xu: investigation, analyses, data curation, and writing (original draft, review, and editing). Lidong Cao: supervision, conceptualization, writing (review and editing), and resources. Tingting Liu: investigation. Huiping Chen: investigation. Yuanbo Li: supervision, conceptualization, writing (review and editing), and resources.

Funding

The authors acknowledge financial support of this work by the National Natural Science Foundation of China (32202368), China Postdoctoral Science Foundation (2022T150713), and Key Laboratory of Tobacco Pest Monitoring and Integrated Management in Tobacco Industry (KLTPMIMT2022-13).

Conflicts of interest

There are no conflicts of interest to declare.

References

1 A. Avellan, J. Yun, B. P. Morais, E. T. Clement, S. M. Rodrigues and G. V. Lowry, Critical review: Role of inorganic nanoparticle properties on their foliar uptake and in planta translocation, *Environ. Sci. Technol.*, 2021, **55**, 13417–13431.
2 C. Mbow, C. Rosenzweig, L. G. Barioni, T. G. Benton, M. Herrero, M. Krishnapillai, E. Liwenga, P. Pradhan, M.-G. Rivera-Ferre and T. Sapkota, *Climate change and land*, 2019, pp. 437–550.
3 X. Zhao, H. Cui, Y. Wang, C. Sun, B. Cui and Z. Zeng, Development strategies and prospects of nano-based smart pesticide formulation, *J. Agric. Food Chem.*, 2018, **66**, 6504–6512.
4 K. Fukamachi, Y. Konishi and T. Nomura, Disease control of phytophthora infestans using cyazofamid encapsulated in poly lactic-co-glycolic acid (PLGA) nanoparticles, *Colloids Surf., A*, 2019, **577**, 315–322.
5 P. L. Wu, P. S. Wang, M. Y. Gu, J. Xue and X. L. Wu, Human health risk assessment of pesticide residues in honeysuckle samples from different planting bases in China, *Sci. Total Environ.*, 2020, **759**, 142747.
6 G. V. Lowry, A. Avellan and L. M. Gilbertson, Opportunities and challenges for nanotechnology in the agri-tech revolution, *Nat. Nanotechnol.*, 2019, **14**, 517–522.
7 M. Kah, N. Tufenkji and J. C. White, Nano-enabled strategies to enhance crop nutrition and protection, *Nat. Nanotechnol.*, 2019, **14**, 532–540.
8 L. Zhao, T. Bai, H. Wei, J. L. Gardea-Torresdey, A. Keller and J. C. White, Nanobiotechnology-based strategies for enhanced crop stress resilience, *Nat. Food*, 2022, **3**, 829–836.
9 N. Li, C. Sun, J. Jiang, A. Wang, C. Wang, Y. Shen, B. Huang, C. An, B. Cui, X. Zhao, C. Wang, F. Gao, S. Zhan, L. Guo, Z. Zeng, L. Zhang, H. Cui and Y. Wang, Advances in controlled-release pesticide formulations with improved efficacy and targetability, *J. Agric. Food Chem.*, 2021, **69**, 12579–12597.
10 D. Wang, N. B. Saleh, A. Byro, R. G. Zepp, E. Sahle-Demessie, T. P. Luxton, K. T. Ho, R. M. Burgess, M. Flury, J. C. White and C. Su, Nano-enabled pesticides for sustainable agriculture and global food security, *Nat. Nanotechnol.*, 2022, **17**, 347–360.

11 Y. Vasseghian, P. Arunkumar, S.-W. Joo, L. Gnanasekaran, H. Kamyab, S. Rajendran, D. Balakrishnan, S. Chelliapan and J. J. Klemeš, Metal-organic framework-enabled pesticides are an emerging tool for sustainable cleaner production and environmental hazard reduction, *J. Cleaner Prod.*, 2022, **373**, 133966.

12 M. C. Camara, E. V. R. Campos, R. A. Monteiro, A. D. E. S. Pereira and L. F. Fraceto, Development of stimuli-responsive nano-based pesticides: emerging opportunities for agriculture, *J. Nanobiotechnol.*, 2019, **17**, 100.

13 C.-Y. Wang, Y.-Q. Liu, C. Jia, M.-Z. Zhang, C.-L. Song, C. Xu, R. Hao, J.-C. Qin and Y.-W. Yang, An integrated supramolecular fungicide nanoplatform based on pH-sensitive metal–organic frameworks, *Chin. Chem. Lett.*, 2023, **34**, 108400.

14 D. Xiao, H. Wu, Y. Zhang, J. Kang, A. Dong and W. Liang, Advances in stimuli-responsive systems for pesticides delivery: Recent efforts and future outlook, *J. Controlled Release*, 2022, **352**, 288–312.

15 J. Zhou, G. Liu, Z. Guo, M. Wang, C. Qi, G. Chen, Xi. Huang, S. Yan and D. Xu, Stimuli-responsive pesticide carriers based on porous nanomaterials: a review, *Chem. Eng. J.*, 2023, **455**, 140167.

16 S. Sharma, B. K. Sahu, L. Cao, P. Bindra, K. Kaur, M. Chandel, N. Koratkar, Q. Huang and V. Shanmugam, Porous nanomaterials: Main vein of agricultural nanotechnology, *Prog. Mater. Sci.*, 2021, **121**, 100812.

17 J. Yang, D. Dai, Z. Cai, Y.-Q. Liu, J.-C. Qin, Y. Wang and Y.-W. Yang, MOF-based multi-stimuli-responsive supramolecular nanoplatform equipped with macrocycle nanovalves for plant growth regulation, *Acta Biomater.*, 2021, **134**, 664–673.

18 Y. Cui, B. Li, H. He, W. Zhou, B. Chen and G. Qian, Metal-organic frameworks as platforms for functional materials, *Acc. Chem. Res.*, 2016, **49**, 483–493.

19 Y. Wang, J. Yan, N. Wen, H. Xiong, S. Cai, Q. He, Y. Hu, D. Peng, Z. Liu and Y. Liu, Metal-organic frameworks for stimuli-responsive drug delivery, *Biomaterials*, 2020, **230**, 119619.

20 J. Yang, D. Dai, X. Zhang, L. Teng, L. Ma and Y.-W. Yang, Multifunctional metal-organic framework (MOF)-based nanoplatforms for cancer therapy: From single to combination therapy, *Theranostics*, 2023, **13**, 295–323.

21 C.-Y. Wang, J. Yang, J.-C. Qin and Y.-W. Yang, Eco-friendly nanoplatforms for crop quality control, protection, and nutrition, *Adv. Sci.*, 2021, **8**, 2004525.

22 C.-Y. Wang, J.-C. Qin and Y.-W. Yang, Multifunctional metal –mrganic framework (MOF)-based nanoplatforms for crop protection and growth promotion, *J. Agric. Food Chem.*, 2023, **71**, 5953.

23 S. Rojas, A. Rodríguez-Diéguez and P. Horcajada, Metal–organic frameworks in agriculture, *ACS Appl. Mater. Interfaces*, 2022, **14**, 16983–17007.

24 J. Yang, C. A. Trickett, S. B. Alahmadi, A. S. Alshammari and O. M. Yaghi, Calcium L-Lactate frameworks as naturally degradable carriers for pesticides, *J. Am. Chem. Soc.*, 2017, **139**, 8118–8121.

25 W. Liang, Z. Xie, J. Cheng, D. Xiao, Q. Xiong, Q. Wang, J. Zhao and W. Gui, A light-triggered pH-responsive metal-organic framework for smart delivery of fungicide to control sclerotinia diseases of oilseed rape, *ACS Nano*, 2022, **15**, 6987–6997.

26 S. Ma, Y. Ji, Y. Dong, S. Chen, Y. Wang and S. Lü, An environmental-friendly pesticide-fertilizer combination fabricated by in-situ synthesis of ZIF-8, *Sci. Total Environ.*, 2021, **789**, 147845.

27 D. Wang, J. Zhou, R. Shi, H. Wu, R. Chen, B. Duan, G. Xia, P. Xu, H. Wang, S. Zhou, C. Wang, H. Wang, Z. Guo and Q. Chen, Biodegradable core-shell dual-metal- organic-frameworks nanotheranostic agent for multiple imaging guided combination cancer therapy, *Theranostics*, 2017, **7**, 4605–4617.

28 B. Russell, J. Villaroel, K. Sapag and A. D. Migone, O_2 Adsorption on ZIF-8: Temperature dependence of the gate-opening transition, *J. Phys. Chem. C*, 2014, **118**, 28603–28608.

29 S. Sun, Z. Yang, J. Cao, Y. Wang and W. Xiong, Copper-doped ZIF-8 with high adsorption performance for removal of tetracycline from aqueous solution, *J. Solid State Chem.*, 2020, **285**, 121219.

30 O. Maan, P. Song, N. Chen and Q. Lu, An in situ procedure for the preparation of zeolitic imidazolate framework-8 polyacrylamide hydrogel for adsorption of aqueous pollutants, *Adv. Mater. Interfaces*, 2019, **6**, 1801895.

31 A. Elaouni, M. El Ouardi, M. Zbair, A. BaQais, M. Saadi and H. A. Ahsaine, ZIF-8 metal organic framework materials as a superb platform for the removal and photocatalytic degradation of organic pollutants: A review, *RSC Adv.*, 2022, **12**, 31801–31817.

32 H. Zhao, Y. Zhao and D. Liu, pH and H_2S dual-responsive magnetic metal-organic frameworks for controlling the release of 5-fluorouracil, *ACS Appl. Bio Mater.*, 2021, **4**, 7103–7110.

33 J. R. Lamichhane, E. Osdaghi, F. Behlau, J. Köhl, J. B. Jones and J. N. Aubertot, Thirteen decades of antimicrobial copper compounds applied in agriculture. A review, *Agron. Sustainable Dev.*, 2018, **38**, 28.

34 C. Xu, Y. Shan, B. Muhammad, B. Xu, L. Cao and Q. Huang, Copper ions chelated mesoporous silica nanoparticles via dopamine chemistry for controlled pesticide release regulated by coordination bonding, *Chem. Eng. J.*, 2020, **395**, 125093.

35 L. Pan, J. Sun, X. Chris Le and L. Zhu, Effect of copper on the translocation and transformation of polychlorinated biphenyls in rice, *Chemosphere*, 2018, **193**, 514–520.

36 J. Chen, X. Xia, S. Chu, H. Wang, Z. Zhang, N. Xi and J. Gan, Cation–π interactions with coexisting heavy metals enhanced the uptake and accumulation of polycyclic aromatic hydrocarbons in spinach, *Environ. Sci. Technol.*, 2020, **54**, 7261–7270.

37 H. Wu, P. Hu, Y. Xu, C. Xiao, Z. Chen, X. Liu, J. Jia and H. Xu, Phloem delivery of fludioxonil by plant amino acid transporter-mediated polysuccinimide nanocarriers for

controlling fusarium wilt in banana, *J. Agric. Food Chem.*, 2021, **69**, 2668–2678.

38 R. Hou, Z. Zhang, S. Pang, T. Yang, J. M. Clark and L. He, Alteration of the Nonsystemic Behavior of the Pesticide Ferbam on Tea Leaves by Engineered Gold Nanoparticles, *Environ. Sci. Technol.*, 2016, **50**, 6216–6223.

39 Z. Wang, J. Niu, C. Zhao, X. Wang, J. Ren and X. Qu, A bimetallic Metal–Organic Framework encapsulated with DNAzyme for intracellular drug synthesis and self-sufficient gene therapy, *Angew. Chem., Int. Ed.*, 2021, **60**, 12431–12437.

40 OECD, *Test No. 203: Fish, Acute Toxicity Test*, OECD Publishing, 2006.

41 K. C. Hyland, A. C. Blaine and C. P. Higgins, Accumulation of contaminants of emerging concern in food crops-part 2: Plant distribution, *Environ. Toxicol. Chem.*, 2015, **34**, 2222–2230.

42 S. Wang, R. Li, F. Dong, Y. Zheng and Y. Li, Determination of a novel pesticide cyetpyrafen and its two main metabolites in crops, soils and water, *Food Chem.*, 2023, **400**, 134049.

43 Y. Wu and Z. Ke, Novel Cu-doped zeolitic imidazolate framework-8 membranes supported on copper foam for highly efficient catalytic wet peroxide oxidation of phenol, *Mater. Today Chem.*, 2022, **24**, 100787.

44 N. Nagarjun and A. Dhakshinamoorthy, A Cu-doped ZIF-8 metal organic framework as a heterogeneous solid catalyst for aerobic oxidation of benzylic hydrocarbons, *New J. Chem.*, 2019, **43**, 18702.

45 U. P. N. Tran, K. K. A. Le and N. T. S. Phan, Expanding applications of metal organic frameworks: Zeolite imidazolate framework ZIF-8 as an efficient heterogeneous catalyst for the Knoevenagel reaction, *ACS Catal.*, 2011, **1**, 120–127.

46 Z. Xie, S. Liang, X. Cai, B. Ding, S. Huang, Z. Hou, P. Ma, Z. Cheng and J. Lin, O_2-Cu/ZIF-8@Ce6/ZIF-8@F127 composite as a tumor microenvironment-responsive nanoplatform with enhanced photo-/chemodynamic antitumor efficacy, *ACS Appl. Mater. Interfaces*, 2019, **11**, 31671–31680.

47 Y. Ma, R. Zhao, H. Shang, S. Zhen, L. Li, X. Guo, M. Yu, Y. Xu, J. Feng and X. Wu, pH-responsive ZIF-8-based metal –organic-framework nanoparticles for termite control, *ACS Appl. Nano Mater.*, 2022, **5**, 11864–11875.

48 C. Zhang, Z. Shu, H. Sun, L. Yan, C. Peng, Z. Dai, L. Yang, L. Fan and Y. Chu, Cu(II)@ZIF-8 nanoparticles with dual enzyme-like activity bound to bacteria specifically for efficient and durable bacterial inhibition, *Appl. Surf. Sci.*, 2011, **611**, 155599.

49 C. Avci, J. Ariñez-Soriano, A. Carné-Sánchez, V. Guillerm, C. Carbonell, I. Imaz and D. Maspoch, Post-synthetic anisotropic wet-chemical etching of colloidal sodalite ZIF cystals, *Angew. Chem., Int. Ed.*, 2015, **54**, 14417–14421.

50 W. Jiang, H. Zhang, J. Wu, G. Zhai, Z. Li, Y. Luan and S. Garg, CuS@MOF-based well-designed quercetin delivery system for chemo-photothermal therapy, *ACS Appl. Mater. Interfaces*, 2018, **10**, 34513–34523.

51 X. Zhang, X. Tang, C. Zhao, Z. Yuan, D. Zhang, H. Zhao, N. Yang, K. Guo, Y. He, Y. He, J. Hu, L. He, L. He and K. Qian, A pH-responsive MOF for site-specific delivery of fungicide to control citrus disease of Botrytis cinerea, *Chem. Eng. J.*, 2022, **431**, 133351.

52 P. L. Ritger and N. A. Peppas, A simple equation for description of solute release II. Fickian and anomalous release from swellable devices, *J. Controlled Release*, 1987, **5**, 37–42.

53 J. Merhej, F. Richard-Forget and C. Barreau, The pH regulatory factor Pac1 regulates Tri gene expression and trichothecene production in Fusarium graminearum, *Fungal Genet. Biol.*, 2011, **48**, 275–284.

54 P. Miralles, T. L. Church and A. T. Harris, Toxicity, uptake, and translocation of engineered nanomaterials in vascular plants, *Environ. Sci. Technol.*, 2012, **46**, 9224–9239.

55 P. Cervantes-Avilés, X. Huang and A. A. Keller, Dissolution and aggregation of metal oxide nanoparticles in root exudates and soil leachate: Implications for nanoagrochemical application, *Environ. Sci. Technol.*, 2021, **55**, 13443–13451.

56 H. Shang, H. Guo, C. Ma, C. Li, B. Chefetz, T. Polubesova and B. Xing, Maize (Zea mays L.) root exudates modify the surface chemistry of CuO nanoparticles: Altered aggregation, dissolution and toxicity, *Sci. Total Environ.*, 2019, **690**, 502–510.

57 C. Deng, Y. Wang, G. Navarro, Y. Sun, K. Cota-Ruiz, J. A. Hernandez-Viezcas, G. Niu, C. Li, J. C. White and J. Gardea-Torresdey, Copper oxide (CuO) nanoparticles affect yield, nutritional quality, and auxin associated gene expression in weedy and cultivated rice (Oryza sativa L.) grains, *Sci. Total Environ.*, 2022, **810**, 152260.

58 P. K. Tiwari, Shweta, A. K. Singh, V. P. Singh, S. M. Prasad, N. Ramawat, D. K. Tripathi, D. K. Chauhan and A. K. Rai, Liquid assisted pulsed laser ablation synthesized copper oxide nanoparticles (CuO-NPs) and their differential impact on rice seedlings, *Ecotoxicol. Environ. Saf.*, 2019, **176**, 321–329.

59 C. Deng, Y. Wang, J. M. Cantu, C. Valdes, G. Navarro, K. Cota-Ruiz, J. A. Hernandez-Viezcas, C. Li, W. H. Elmer, C. O. Dimkpa, J. C. White and J. L. Gardea-Torresdey, Soil and foliar exposure of soybean (Glycine max) to Cu: Nanoparticle coating-dependent plant responses, *NanoImpact*, 2022, **26**, 100406.

60 Y. Wang, C. Dimkpa, C. Deng, W. H. Elmer, J. Gardea-Torresdey and C. White, Impact of engineered nanomaterials on rice (Oryza sativa L.): A critical review of current knowledge, *Environ. Pollut.*, 2022, **297**, 118738.

